

Spontaneous magnetostriction effects in the chiral magnet CrNb_3S_6

Takayuki Tajiri,¹ Masaki Mito,^{2,3,*} Yusuke Kousaka,^{3,4} Jun Akimitsu,⁵ Jun-ichiro Kishine,^{3,6} and Katsuya Inoue^{3,7,8}

¹*Faculty of Science, Fukuoka University, Fukuoka 814-0180, Japan*

²*Faculty of Engineering, Kyushu Institute of Technology, Kitakyushu 804-8550, Japan*

³*Chirality Research Center, Hiroshima University, Higashihiroshima 739-8526, Japan*

⁴*Graduate School of Engineering, Osaka Prefecture University, Sakai 599-8570, Japan*

⁵*Research Institute for Interdisciplinary Science, Okayama University, Okayama 700-8530, Japan*

⁶*Graduate School of Arts and Sciences, The Open University of Japan, Chiba 261-8586, Japan*

⁷*Graduate School of Science, Hiroshima University, Higashihiroshima 739-8526, Japan*

⁸*Institute for Advanced Materials Research, Hiroshima University, Higashihiroshima 739-8526, Japan*



(Received 15 April 2020; revised 3 June 2020; accepted 8 July 2020; published 27 July 2020)

We identified the spontaneous magnetostriction effects in the chiral magnet CrNb_3S_6 with the Dzyaloshinskii-Moriya interaction. The powdered x-ray diffraction patterns indicate a prominent magnetostriction effect at the earth field. The unit-cell volume remains almost constant, as in the so-called Invar effect, below 170 K in the paramagnetic region, where the atomic positions of Nb and S show characteristic changes. Below the magnetic ordering temperature of 127 K, the lattice constants a and c exhibit an opposite temperature dependence. When a finite magnetic field of 1.2 kOe is applied, a magnetostriction appears that counterbalances the spontaneous magnetostriction. The magnetostriction phenomena in CrNb_3S_6 were investigated from the viewpoint of the atomic level of the chiral effect.

DOI: [10.1103/PhysRevB.102.014446](https://doi.org/10.1103/PhysRevB.102.014446)

I. INTRODUCTION

In a chiral space group without any rotoinversion symmetry elements, crystallographic chirality allows the Dzyaloshinskii-Moriya (DM) interaction, which arises from a combination of second-order perturbation of the spin-orbit coupling (SOC) and the exchange interaction [1,2]. The competition between the DM and exchange interactions stabilizes a long-wavelength helimagnetic (HM) order. In addition, SOC itself often results in magnetostriction. Magnetostriction in chiral magnets has already been studied in a B20 (cubic) type of MnSi through the capacitance measurement [3], where the relation of the magnetostriction to the structural symmetry has been discussed in the point group theory. However, the atomic level of the chiral effect is not considered. This study investigates the magnetostriction phenomena in a typical hexagonal chiral magnet, CrNb_3S_6 , considering lattice deformation on the atomic scale. The change in lattice parameters is related to the change in the local structural symmetry around a magnetic Cr^{3+} ion.

CrNb_3S_6 has a stacked structure of hexagonal NbS_2 layers. The insertion of Cr^{3+} between the NbS_2 layers precludes the inversion symmetry; thus, the material crystallizes in the noncentrosymmetric hexagonal space group $P6_322$ (No. 182) [4–6]. Cr occupies the position of 6S octahedral holes, the $2d$ site ($2/3, 1/3, 1/4$). The Nb positions are classified as the $2a$ site at $(0, 0, 1/2)$ and the $4f$ site at $(2/3, 1/3, z)$, as shown in Fig. 1(a). The atomic position of S, the $12i$ site

(x, y, z) , is a general position. Nb($4f$) is located so it enters the 3S triangle of the CrS_6 octahedron, and the z value of Nb($4f$) is not $1/2$. In this cluster unit of $\text{CrS}_6\text{-Nb}_2$, the local symmetry around Cr is approximately D_{3d} ; thus, the Cr $3d$ orbitals would show an energy splitting $t_{2g} \rightarrow e'_g + a_{1g}$, as shown in Fig. 1(a). The a_{1g} orbital of Cr $3d$ orbitals extends along the c axis toward the Nb($4f$) atoms. The z^2 orbital of Nb($4f$) is hybridized with the delocalized a_{1g} orbital of Cr [7], resulting in the appearance of orbital angular momentum [7] and ferromagnetic interaction [8].

CrNb_3S_6 has a HM ground state with the propagation vector along the c axis [5], and the magnetic ordering temperature T_c of CrNb_3S_6 is 127 K [5,9,10]. According to a Lorenz microscopy experiment, a ferromagnetic network develops on the ab plane [11]. A Monte Carlo simulation was used to estimate the in-plane exchange interaction on the ab plane (67 K) [12]. An electron spin resonance experiment revealed that both the DM interaction and the easy-plane anisotropy appear at approximately 1 K, whereas the interplane exchange interaction occurs at 16 K [13]. A decrease in T_c under hydrostatic pressure is reportedly associated with a decrease in the distortion of the CrS_6 octahedron [9,14]. To date, the physical properties of CrNb_3S_6 have been explained on the basis of structural information at room temperature.

In the monoaxial chiral HM texture, a finite dc magnetic field H perpendicular to the chiral axis stabilizes a chiral soliton lattice (CSL) state, in which the ferromagnetic arrays are connected with kinks [15–17]. The kinks (single discommensurations) are spiral textures with 2π rotation and are treated numerically as solitons. Experimental evidence of the CSL phase was obtained by Lorentz transmission electron

*mitoh@mns.kyutech.ac.jp

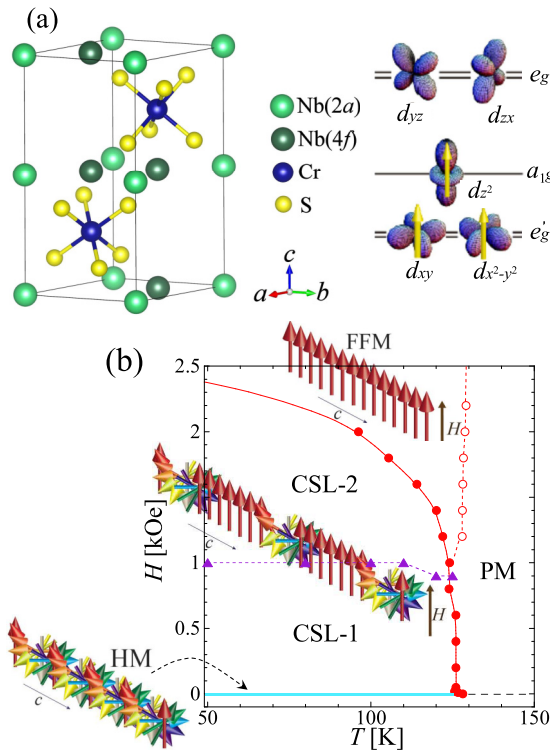


FIG. 1. (a) Crystal structure of CrNb_3S_6 and its $3d$ orbitals. $\text{Nb}(2a)$ and $\text{Nb}(4f)$ are shown in light and dark green, respectively. (b) Phase diagram as a function of temperature T and dc magnetic field H perpendicular to the c axis. When H is scanned from zero, the HM state (light blue) is transformed to a forced-ferromagnetic (FFM) state via a chiral soliton lattice (CSL).

microscopy [11]. The change in the soliton number results in discrete changes in the magnetoresistance [18] and magnetization [19–22]. The phase diagram at $H \perp c$ was verified both experimentally [10,23–27] and theoretically [12,28–30]. The CSL phase is divided into at least two regions [CSL-1 and CSL-2, Fig. 1(b)] depending on irreversibility [10]. The manipulability of the spin texture under H originates from the chirality of the crystal structure, suggesting a strong magnetostructural correlation. It is an open question whether the change in magnetic property with H can influence the crystal structure. Electron diffraction analysis cannot provide an answer based on the crystallography because of insufficient spatial resolution [11]. Thus, to know how H modifies the intrinsic magnetostriction effect in CrNb_3S_6 , we investigate the lattice parameters of a powder sample at $H = 0$ and a single crystal at $H = 0$ and 1.2 kOe (both $H \perp c$ and $H//c$) as a function of T .

The change in structural symmetry changes the distribution of the orbital wave function of electrons, so that the resultant change in SOC brings about the change in spin alignment. The present study investigates how structural change in the atomic level occurs by the change in spin alignment by reducing thermal fluctuation and applying a magnetic field. It is not just a magnetostriction study from the macroscopic viewpoint but an experimental study to investigate the effect of SOC from the atomic level of structural analyses.

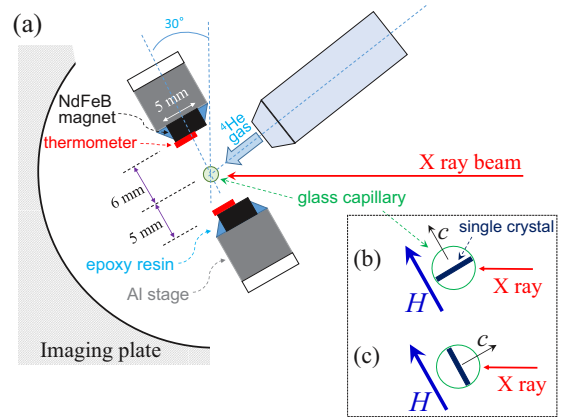


FIG. 2. (a) Setup of XRD experiments at $H = 1.2$ kOe. H was obtained using two facing NdFeB magnets with opposite magnetizations. The sample was cooled to 90 K, which was the lower limit at which the temperature of the NdFeB magnets was maintained above 280 K. The setups using a single crystal for (b) $H//c$ and (c) $H \perp c$.

II. EXPERIMENTAL METHODS

We performed x-ray diffraction (XRD) analyses as a function of T using a synchrotron radiation system with a cylindrical imaging plate at the Photon Factory at the Institute of Materials Structure Science of the High Energy Accelerator Research Organization [31]. The energy of the incident x rays was 16 keV. The experimental setup for $H = 1.2$ kOe using two permanent magnets is shown in Fig. 2. Two NdFeB magnets (NeoMag, N48H) with a remanence of 13.8 kG and dimensions of $10 \times 6 \times 3$ mm³ were used to produce the 1.2-kOe field. The remanence of a NdFeB magnet depends on its temperature. The temperature of the magnets was measured using a K-type chromel-alumel thermocouple. During the XRD measurements, the sample temperature T was increased from 92.8 to 294.7 K so that the temperature of the magnets was held at 289.2–298.2 K to maintain H . Consequently, the H value at the sample position is calculated at room temperature. The actual T sequence at $H = 1.2$ kOe corresponds to paramagnetic (PM) → forced-ferromagnetic (FFM) → CSL-2 → FFM → PM for $H//ab$ and PM → conical magnetic (CM) → PM for $H//c$.

The powder sample and single crystal of CrNb_3S_6 were synthesized using a procedure described elsewhere [11]. The powder sample had already been used in a hydrostatic pressure experiment [9]. First, we conducted the powder XRD measurement at $H = 0$. The diffraction patterns were analyzed by Rietveld refinement using the REITAN-FP package [32]. Next, we performed the XRD experiments using the single crystal at $H = 0$ and 1.2 kOe. We prepared a magnetic field with both $H//ab$ ($H \perp c$) and $H//c$. To evaluate the lattice parameters, we used 14 ($hk3$) and 11 ($hk2$) spots for the $H//ab$ setup and 4 ($21l$), 4 ($20l$), and 7 ($11l$) spots for the $H//c$ setup. The words “shrinkage,” “elongation,” and “expansion” are used to describe structural changes with increasing temperature.

The T dependence of magnetization M at $H = 1.2$ kOe was observed using a commercial superconducting quantum interference device magnetometer to confirm the M values and

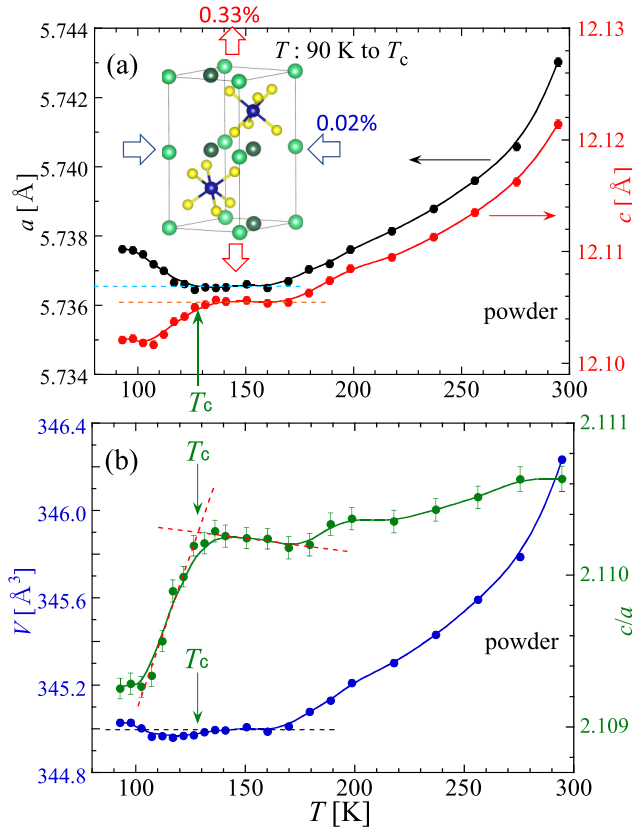


FIG. 3. Lattice parameters a , c , V , and c/a of CrNb_3S_6 at $H = 0$ as estimated by Rietveld analysis. The data for a and c are shown in (a), and those for V and c/a are shown in (b). Green arrows indicate the T_c value confirmed by ac magnetization at zero field [9,14].

the magnetic irreversibility between field-cooling and field-warming processes. Then, the c axis of the single crystal was placed in the direction parallel to H or perpendicular to H . For $H//ab$ ($H \perp c$), ac magnetization in the field-cooling process at an ac field with an amplitude of 3.86 Oe and a frequency of 10 Hz was measured to identify a series of field-induced transition temperatures. The minimum T (80 K) was lower than that in the XRD experiment. At room temperature, H was increased to 1.2 kOe. Then, M was measured in the cooling process to 80 K; this was followed by its measurement in the warming process from 80 K. The obtained information is helpful to understand the conditions of the XRD experiment using the single crystal, from the viewpoint of magnetizing.

III. EXPERIMENTAL RESULTS AND DISCUSSION

A. Under zero magnetic field

Figures 3(a) and 3(b) show the lattice constants a and c , their ratio c/a , and the unit cell volume V of CrNb_3S_6 at $H = 0$. Ordinal thermal shrinkage appears in the paramagnetic region above 170 K. As shown in the next section, the development of M at a finite H owing to the short-range order is dominant below 170 K. For 130–170 K, all of the lattice parameters change very little, suggesting a type of Invar effect due to competition between the thermal expansion and magnetic shrinkage. Here, c/a was kept nearly constant [see Fig. 3(b)]. For $T < 130$ K, the a axis shrinks by 0.02%, and

the c axis becomes 0.33% longer, resulting in a prominent change in c/a [see Fig. 3(b)]. Consequently, V tends to have an almost constant value (indeed, slightly decreased), even for $T < 130$ K. There, the decrease in volume due to the shrinkage of the easy plane is offset by the increase in V due to the elongation along the hard axis (c axis). Thus, this behavior below T_c , which is opposite to thermal expansion, is identified as spontaneous “magnetostriction” associated with the HM order.

Figures 4(a)–4(d) illustrate these phenomena in terms of the atomic coordinates $\text{Nb}(4f)_z$, S_x , S_y , and S_z for CrNb_3S_6 at $H = 0$, respectively. The z coordinate of $\text{Nb}(4f)$, $\text{Nb}(4f)_z$, exhibits characteristic changes at 130, 180, and 260 K, where the change at 130 K is associated with the HM order. Under hydrostatic pressure, $\text{Nb}(4f)_z$ approaches 0.5 for $\text{Nb}(2a)$ [9]. The thermal shrinkage for $T > T_c$ and hydrostatic compression have similar effects on $\text{Nb}(4f)_z$. Thus, the symmetry of the CrS_6 octahedron approaches that of the regular octahedron in both cases, as described later. Herein, it is noted that all of the atomic coordinates of S (S_x , S_y , and S_z) exhibit a change at T_c , similar to $\text{Nb}(4f)_z$. The characteristic temperatures that determine the changes in S_x , S_y , and S_z except for T_c are not uniform. Of the three atomic coordinates of S, the characteristic temperatures for S_z , such as 130, 190, and 240 K, are particularly close to those in $\text{Nb}(4f)_z$, suggesting interlocking motion between $\text{Nb}(4f)$ and S atoms.

To know the change in the structural symmetry of the CrS_6 octahedron, we have to study the change in bonding angles, such as $\angle\text{S1CrS4}$ and $\angle\text{S5CrS6}$, as shown in Fig. 5. Herein, $\angle\text{S1CrS4}$ is equal to $\angle\text{S2CrS5}$ and $\angle\text{S3CrS6}$. Further, $\angle\text{S5CrS6}$ is equal to $\angle\text{S1CrS2}$, $\angle\text{S1CrS3}$, $\angle\text{S2CrS3}$, $\angle\text{S4CrS5}$, and $\angle\text{S4CrS6}$. In the regular octahedron, $\angle\text{S1CrS4} = 180^\circ$, and $\angle\text{S5S1S6} = \angle\text{S3S1S5} = \angle\text{S2S1S6} = 60^\circ$. As suggested by the interlocking motion between $\text{Nb}(4f)$ and S atoms in Fig. 4, the change in the structural symmetry of the CrS_6 octahedron is related to the displacement of $\text{Nb}(4f)$ along the c axis, as illustrated in Fig. 5(a). The distortion of two regular triangles, S4S5S6 and S1S2S3 , was monitored with the angle $\angle\text{S1CrS4}$ [see Fig. 5(b)]. The increase and decrease in $\angle\text{S5CrS6}$ represent the elongation and contraction of the CrS_6 octahedron along a direction parallel to the ab plane, respectively [see Fig. 5(c)]. The Cr network on the ab plane constructs the ferromagnetic spin alignment, which is strengthened by the easy-plane type of the magnetic anisotropy. The bonding length S1–S2 reflects the size of the regular triangle length of S1S2S3 , while the changes in both S1–S5 and S1–S6 reflect the distortion between two SSS regular triangles.

Figure 6(a) shows the T dependence of $\angle\text{S1CrS4}$ and $\angle\text{S5CrS6}$. First, $\angle\text{S1CrS4}$ has the lowest value around T_c and another minimum at approximately 220 K. At approximately T_c , the CrS_6 octahedron has the largest distortion. Thus, in the T region from 90 to 300 K, the octahedron distortion repeats the up-and-down pattern twice. Next, $\angle\text{S5CrS6}$ exhibits the constant-down-up-down pattern with increasing T : Below 140 K, $\angle\text{S5CrS6}$ keeps the maximum value at approximately 88° . This originates from the stabilization of the ferromagnetic alignment on the ab plane. In the paramagnetic region above 140 K, the CrS_6 octahedron exhibits the contraction, elongation, and contraction progression along the direction

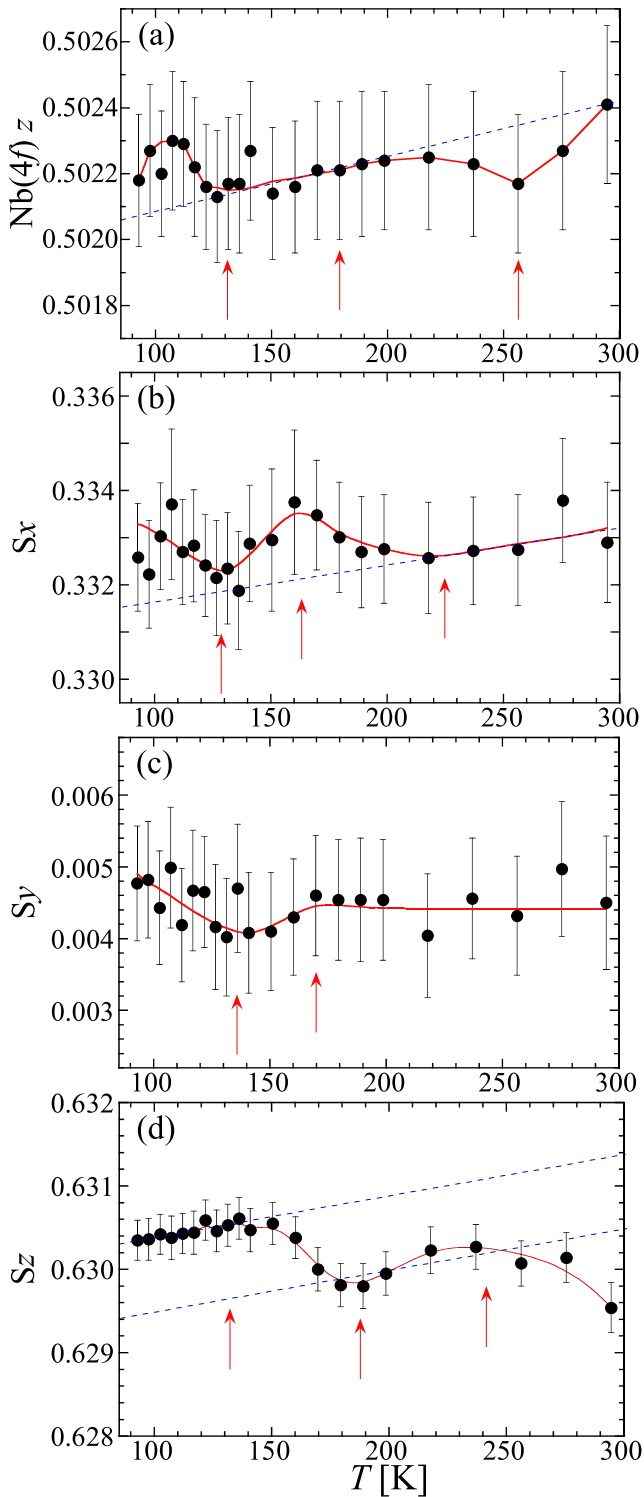


FIG. 4. T dependences of atomic coordinates such as (a) $\text{Nb}(4f)_z$, (b) S_x , (c) S_y , and (d) S_z . The characteristic temperatures are indicated by red arrows, and the dashed lines are guides for viewing their trends.

on the ab plane. The series of characteristic temperatures for the change in $\angle\text{S5CrS6}$ are slightly higher than those for $\angle\text{S1CrS4}$. Furthermore, their T dependences may be influenced by the z coordinate of $\text{Nb}(4f)$.

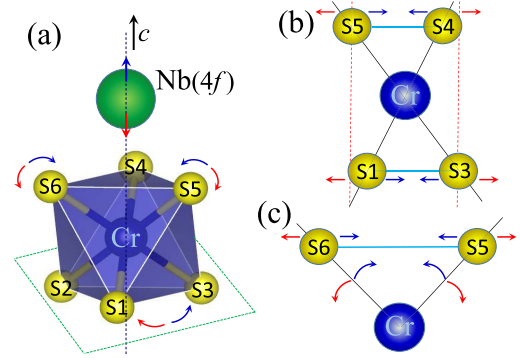


FIG. 5. (a) Local structure of the CrS_6 octahedron located at the downside of $\text{Nb}(4f)$. $\angle\text{S1CrS4} = \angle\text{S2CrS5}$, $\angle\text{S3CrS6}$, $\angle\text{S5CrS6} = \angle\text{S1CrS2}$, $\angle\text{S1CrS3}$, $\angle\text{S2CrS3}$, $\angle\text{S4CrS5}$, $\angle\text{S4CrS6}$. Two triangles such as S1S2S3 and S4S5S6 are regular triangles. (b) Structural distortion between two regular triangles presented with $\angle\text{S1CrS4}$, which slightly deviates from 180° . (c) Elongation and/or contraction of the CrS_6 octahedron along a direction parallel to the ab plane, illustrated with the change in $\angle\text{S5CrS6}$. In (a)–(c), the trends in local atomic motion with the up and down motions of $\text{Nb}(4f)$ are illustrated with blue and red arrows, respectively. The green dotted lines in (a) show the plane including the regular triangle S1S2S3 . Red and blue arrows in the plane present the direction of the rotation of the regular triangle S1S2S3 .

Figure 6(b) shows the T dependence of $\angle\text{S5S1S6}$, $\angle\text{S3S1S5}$, and $\angle\text{S2S1S6}$. Among these three SSS angles, $\angle\text{S5S1S6}$ and $\angle\text{S2S1S6}$ exhibit the same T dependence as $\angle\text{S5CrS6}$ and $\angle\text{S1CrS4}$, respectively. The aforementioned phenomena of the change in the structural symmetry of CrS_6 octahedron can also be traced with $\angle\text{S5S1S6}$ and $\angle\text{S2S1S6}$.

Figure 6(c) shows bonding lengths such as S1–S2 , S1–S5 , and S1–S6 as a function of T . S1–S5 and S1–S6 also exhibit a T dependence similar to those of $\angle\text{S2S1S6}$ and $\angle\text{S3S1S5}$, respectively. S1–S2 has a minimum at approximately 160 K, which is close to the high- T limit exhibiting the Invar effect, and the size of the regular triangle S1S2S3 is minimum in the paramagnetic region. The change in $\angle\text{S1CrS4}$ shown in Fig. 6(a) reveals that the minimizing in the regular triangle size is related to the decrease in the distortion of the CrS_6 octahedron.

Thus, all angles $\angle\text{S1CrS4}$, $\angle\text{S5CrS6}$, $\angle\text{S5S1S6}$, $\angle\text{S3S1S5}$, and $\angle\text{S2S1S6}$ and the bond lengths S1–S2 , S1–S5 , and S1–S6 change at T_c . The changes in the structural symmetry of the CrS_6 octahedron, specifically the change along the directions parallel to the ab plane and distortion of two SSS regular triangles, can be phenomenologically related to the change in the z coordinates of $\text{Nb}(4f)$. In brief, the Invar effects below 170 K are associated with the change in the symmetry of the CrS_6 octahedron. At 170 K, the distortion of the CrS_6 octahedron becomes the minimum. At T_c , the CrS_6 octahedron is most distorted. For reference, the crystal structure at $T = 90$ K is almost the same as that at room temperature.

B. Under a magnetic field of 1.2 kOe

Figures 7(a) and 7(b) show the T dependence of magnetization M at $H = 1.2$ kOe for $H//ab$ and $H//c$, respectively.

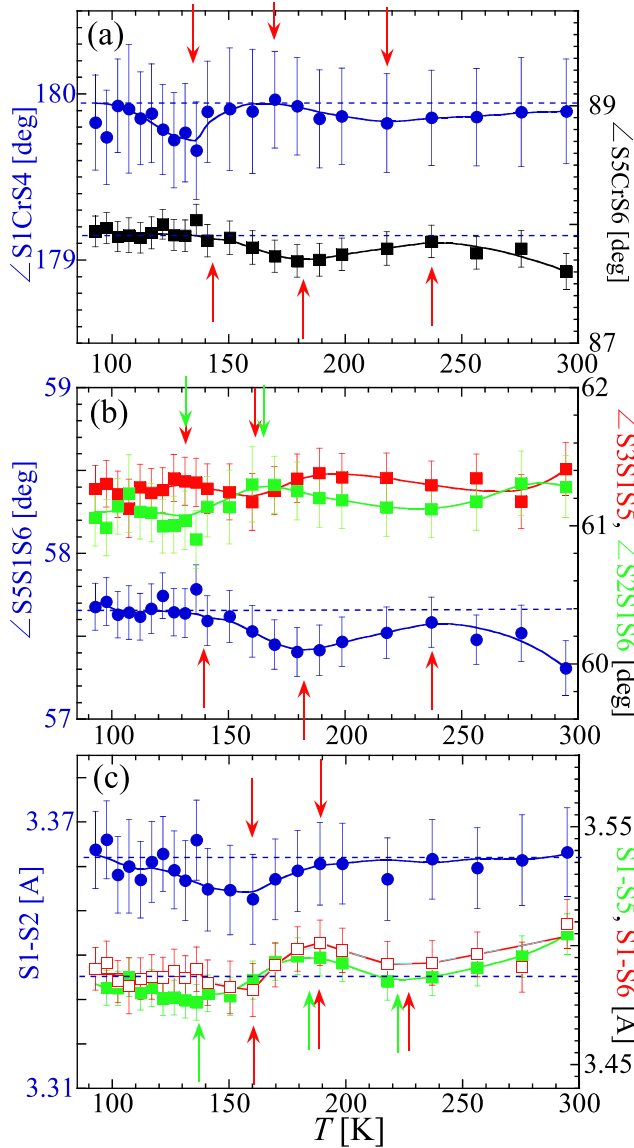


FIG. 6. T dependences of (a) bonding angles $\angle S1CrS4$ and $\angle S5CrS6$, (b) bonding angles $\angle S5S1S6$, $\angle S3S1S5$, and $\angle S2S1S6$, and (c) bonding lengths $S1-S2$, $S1-S5$, and $S1-S6$. The characteristic temperatures are indicated by red arrows, and the dashed lines are base lines for viewing their trends.

In Fig. 7(a), the data for the in-phase ac magnetization m' observed in the field-cooling process at $H = 1.2$ kOe are also shown. In Ref. [10], it was found that in the warming process after zero-field cooling, CSL-2 transforms to PM via FFM at $H = 1.2$ kOe. The present m' data identify that three phases exist independently of the cooling manner such as field cooling or zero-field cooling. Figure 7(b) exhibits the transformation of CM to PM from the low- T side, and the order of M is one tenth of that for $H//ab$. In both cases, small hysteresis was observed between field cooling and field warming. The XRD data conducted under the same field-cooling circumstance are presented below.

Figure 8 shows the lattice parameters a , c , and V estimated experimentally using the single crystal at $H = 0$ and $H = 1.2$ kOe for $H//ab$ [Figs. 8(a)–8(c)] and $H//c$ [Figs. 8(e)–

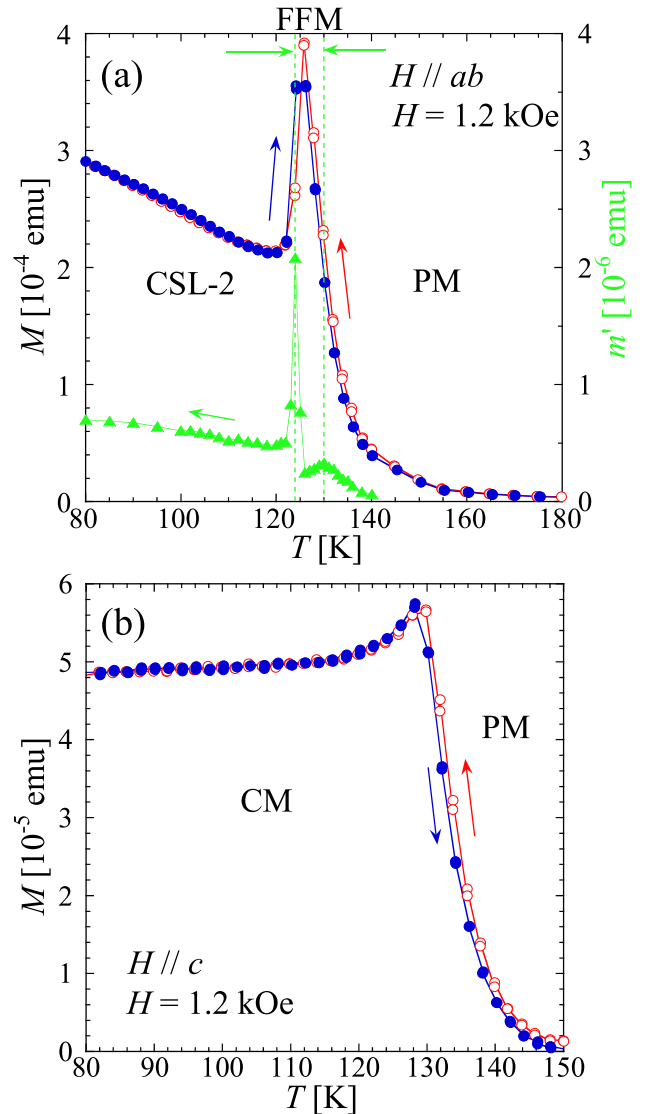


FIG. 7. T dependence of magnetization M at $H = 1.2$ kOe for (a) $H//ab$ and (b) $H//c$. Red and blue indicate data obtained during field cooling and field warming, respectively. For $H//ab$, in-phase ac magnetization m' observed in the field-cooling process at the ac field with an amplitude of 3.86 Oe and frequency of 10 Hz is plotted with green triangles. A phase transformation is identified as CSL-2 \rightarrow FFM \rightarrow PM phases for the low- T side. For $H//c$, a phase transformation occurs between the CM and PM phases.

8(g)]. For $H//ab$, the decrease in a and increase in c below T_c at $H = 0$ change to an increase in a and a slight decrease in c [Figs. 8(a) and 8(b)]. The changes in the unit cell as T is increased from 90 K to T_c are shown in Fig. 8(d). The lattice constant changes notably with respect to the H direction against the easy plane, and it is understood with an H -induced magnetostriction depending on M^2 . Consequently, V does not change greatly below T_c between $H = 0$ and $H//ab$ [Fig. 8(c)], although the scenario for $H//ab$ is different from that of the spontaneous magnetostriction at $H = 0$.

Next, as seen in Figs. 7(a) and 7(b), the M value for $H//c$ is approximately one tenth that for $H//ab$. Consequently, the expansion of the ab plane below T_c for $H//c$ [0.3%; Fig. 8(h)]

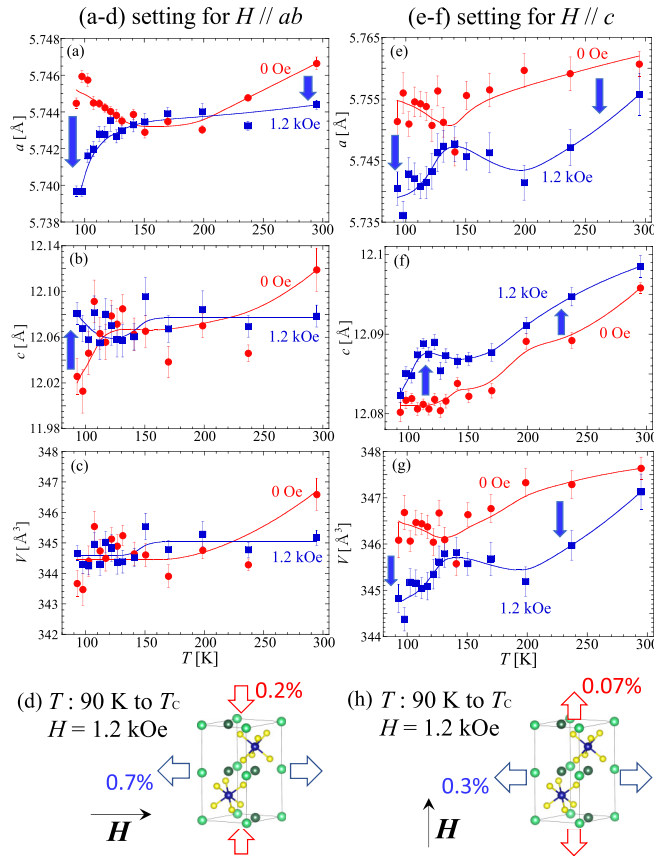


FIG. 8. T dependence of lattice parameters estimated in experiments using a single crystal at $H = 1.2$ kOe for (a)–(c) $H \perp c$ and (e)–(g) $H // c$. (d) and (h) The behavior between 90 K and T_c . For reference, the results at $H = 0$ are also shown.

is smaller than that for $H // ab$ [0.7%; Fig. 8(d)]. For $H // c$, c increases with increasing T below T_c , which is similar to the behavior at $H = 0$. The expansion of the ab plane and elongation along the c axis below T_c [Fig. 8(h)] result in an increase in V , suggesting that applying $H // c$ weakens the

spontaneous magnetostriction. For the application of the $H // c$ field, over the entire T region, the shrinkage of the ab plane is greater than the elongation along the c axis, resulting in a reduction in V . Interestingly, the change in V under the $H // c$ field is suppressed at approximately T_c . Thus, the spontaneous magnetostriction is modified by applying the magnetic field H , and the type of change depends on the direction of H .

IV. CONCLUSION

We observed spontaneous magnetostriction in CrNb_3S_6 . The magnetostriction appears as the so-called Invar effects in two T regions, the PM (130–170 K) and HM (below T_c) regions. The former Invar effect originates from the changes in the symmetry of the CrS_6 octahedron, and there both lattice constants a and c do not change, resulting in no change in the unit-cell volume. The unit-cell volume remains constant also below T_c , where the elongation of the unit cell along the c axis and shrinking of the ab plane are in competition. The Invar effect below T_c originates in the ferromagnetic alignments on the ab planes. This spontaneous magnetostriction was modified by a magnetic field H , and the manner depended on the H direction. Thus, in CrNb_3S_6 with SOC, a prominent magnetostriction effect was observed, and the actual effects are thought to depend on both the magnitude and direction of H . Fortunately, the orbital angular momentum of CrNb_3S_6 was already estimated, and the atomic SOC among the Cr $3d$ and Nb $4d$ were already discussed by the first-principles electronic structure calculations. A discussion of the magnetostriction based on electronic structure is desirable.

ACKNOWLEDGMENTS

This work was supported by a Grant-in-Aid for Scientific Research, Grant No. (S) 25220803, from the Ministry of Education, Culture, Sports, Science and Technology (MEXT), Japan. This work was also supported by the Centre for Chiral Science at Hiroshima University (the MEXT program for promoting the enhancement of research universities, Japan) and the JSPS Core-to-Core Program, A. Advanced Research Networks.

- [1] I. E. Dzyaloshinskii, *J. Phys. Chem. Solid* **4**, 241 (1958).
- [2] T. Moriya, *Phys. Rev.* **120**, 91 (1960).
- [3] S. Wang, Y. Hu, J. Tang, W. Wei, J. Cong, Y. Sun, H. Du, and M. Tian, *New J. Phys.* **21**, 123052 (2019).
- [4] F. Hulliger and E. V. A. Pobitschka, *J. Solid State Chem.* **1**, 117 (1970).
- [5] T. Miyadai, K. Kikuchi, H. Kondo, S. Sakka, M. Arai, and Y. Ishikawa, *J. Phys. Soc. Jpn.* **52**, 1394 (1983).
- [6] L. M. Volkova and D. V. Marinin, *J. Appl. Phys.* **116**, 133901 (2014).
- [7] M. Mito, H. Ohsumi, T. Shishidou, F. Kuroda, M. Weinert, K. Tsuruta, Y. Kotani, T. Nakamura, Y. Togawa, J. Kishine, Y. Kousaka, J. Akimitsu, and K. Inoue, *Phys. Rev. B* **99**, 174439 (2019).
- [8] N. Sirica, P. Vilmercati, F. Bondino, I. Pis, S. Nappini, S. K. Mo, A. V. Fedorov, I. V. P. K. Das, J. Fujii, L. Li *et al.*, *Commun. Phys.* **3**, 65 (2020).
- [9] M. Mito, T. Tajiri, K. Tsuruta, H. Deguchi, J. Kishine, K. Inoue, Y. Kousaka, Y. Nakao, and J. Akimitsu, *J. Appl. Phys.* **117**, 183904 (2015).
- [10] K. Tsuruta, M. Mito, H. Deguchi, J. Kishine, Y. Kousaka, J. Akimitsu, and K. Inoue, *Phys. Rev. B* **93**, 104402 (2016).
- [11] Y. Togawa, T. Koyama, K. Takayanagi, S. Mori, Y. Kousaka, J. Akimitsu, S. Nishihara, K. Inoue, A. S. Ovchinnikov, and J. Kishine, *Phys. Rev. Lett.* **108**, 107202 (2012).
- [12] M. Shinozaki, S. Hoshino, Y. Masaki, J. Kishine, and Y. Kato, *J. Phys. Soc. Jpn.* **85**, 074710 (2016).

- [13] D. Yoshizawa, J. Kishine, Y. Kousaka, Y. Togawa, M. Mito, J. Akimitsu, K. Inoue, and M. Hagiwara, *Phys. Proc.* **75**, 926 (2015).
- [14] M. Mito, S. Tominaga, Y. Komorida, H. Deguchi, S. Takagi, Y. Nakao, Y. Kousaka, and J. Akimitsu, *J. Phys: Conf. Ser.* **215**, 012182 (2010).
- [15] I. E. Dzyaloshinskii, *Zh. Eksp. Teor. Fiz.* **47**, 992 (1964) [*Sov. Phys. JETP* **20**, 665 (1965)].
- [16] J. Kishine, K. Inoue, and Y. Yoshida, *Prog. Theor. Phys. Suppl.* **159**, 82 (2005).
- [17] Y. Togawa, Y. Kousaka, K. Inoue, and J. Kishine, *J. Phys. Soc. Jpn.* **85**, 112001 (2016).
- [18] Y. Togawa, T. Koyama, Y. Nishimori, Y. Matsumoto, S. McVitie, D. McGrouther, R. L. Stamps, Y. Kousaka, J. Akimitsu, S. Nishihara, K. Inoue, I. G. Bostrem, V. E. Sinitzyn, A. S. Ovchinnikov, and J. Kishine, *Phys. Rev. B* **92**, 220412(R) (2015).
- [19] K. Tsuruta, M. Mito, Y. Kousaka, J. Akimitsu, J. Kishine, Y. Togawa, H. Ohsumi, and K. Inoue, *J. Phys. Soc. Jpn.* **85**, 013707 (2016).
- [20] K. Tsuruta, M. Mito, Y. Kousaka, J. Akimitsu, J. Kishine, Y. Togawa, and K. Inoue, *J. Appl. Phys.* **120**, 143901 (2016).
- [21] M. Mito, H. Ohsumi, K. Tsuruta, Y. Kotani, T. Nakamura, Y. Togawa, M. Shinozaki, Y. Kato, J. I. Kishine, J. I. Ohe, Y. Kousaka, J. Akimitsu, and K. Inoue, *Phys. Rev. B* **97**, 024408 (2018).
- [22] M. Ohkuma, M. Mito, N. Nakamura, K. Tsuruta, J. Ohe, M. Shinozaki, Y. Kato, J. Kishine, Y. Kousaka, J. Akimitsu *et al.*, *AIP Adv.* **9**, 075212 (2019).
- [23] Y. Togawa, Y. Kousaka, S. Nishihara, K. Inoue, J. Akimitsu, A. S. Ovchinnikov, and J. Kishine, *Phys. Rev. Lett.* **111**, 197204 (2013).
- [24] N. J. Ghimire, M. A. McGuire, D. S. Parker, B. Sipoş, S. Tang, J.-Q. Yan, B. C. Sales, and D. Mandrus, *Phys. Rev. B* **87**, 104403 (2013).
- [25] E. M. Clements, R. Das, L. Li, P. J. Lampen-Kelley, M.-H. Phan, V. Keppens, D. Mandrus, and H. Srikanth, *Sci. Rep.* **7**, 6545 (2017).
- [26] H. Han, L. Zhang, D. Sapkota, N. Hao, L. Ling, H. Du, L. Pi, C. Zhang, D. G. Mandrus, and Y. Zhang, *Phys. Rev. B* **96**, 094439 (2017).
- [27] E. M. Clements, R. Das, M.-H. Phan, L. Li, V. Keppens, D. Mandrus, M. Osofsky, and H. Srikanth, *Phys. Rev. B* **97**, 214438 (2018).
- [28] V. Laliena, J. Campo, J.-I. Kishine, A. S. Ovchinnikov, Y. Togawa, Y. Kousaka, and K. Inoue, *Phys. Rev. B* **93**, 134424 (2016).
- [29] V. Laliena, J. Campo, and Y. Kousaka, *Phys. Rev. B* **94**, 094439 (2016).
- [30] V. Laliena, J. Campo, and Y. Kousaka, *Phys. Rev. B* **95**, 224410 (2017).
- [31] A. Fujiwara, K. Ishii, T. Watanuki, H. Suematsu, H. Nakao, K. Ohwada, Y. Fujii, Y. Murakami, T. Mori, H. Kawada *et al.*, *J. Appl. Crystallogr.* **33**, 1241 (2000).
- [32] F. Izumi and K. Momma, *Solid State Phenom.* **130**, 15 (2007).